SPE-176603-MS

Dielectric Permittivity Dispersion Measurements in Downhole Conditions – Effect on Porosity Measurements

A. Bondarenko, V. Dorovsky, Yu. Perepechko, and N. Velker, Novosibirsk Technology Center, Baker Hughes;
N. Golikov, Trofimuk Institute of Petroleum Geology and Geophysics (IPGG SB RAS)

This paper was prepared for presentation at the SPE Russian Petroleum Technology Conference held in Moscow, Russia, 26–28 October 2015.

Abstract

The dielectric dispersion of porous media saturated with water and oil is described by the Havriliak–Negami curve in the frequency range 10 kHz – 50 MHz with characteristic values of polarization parameters. Laboratory data show the relationship between porosity and polarization parameters. This relationship allows us to determine porosity of water-and-oil saturated formation under downhole conditions, using borehole dielectric logging methods. In this study, a possibility of using borehole electromagnetic (EM) inductive measurements for determining dispersion of complex dielectric permittivity of the formation, including the invaded zone was investigated. The influence of the inductive measurement error when finding formation porosity when determining polarization parameters of the frequency dependence of complex dielectric permittivity (the Havriliak–Negami spectrum) was studied.

For this study, a vertically oriented coil is placed in the well (along the borehole wall), creating a harmonic electromagnetic field. Several receivers that are aligned with the borehole axis measure this harmonic electromagnetic field. By using the magnetic field values on the well axis, we solve the inverse problem of determining complex dielectric permittivity of the formation, taking into account the invaded zone. Dielectric permittivity of the formation is calculated at different frequencies and is then used to restore the frequency dispersion curve, which enables us to find polarization parameters for the Havriliak-Negami polarization curve, taking into account the measurement error. Subsequently, these parameters can be used to find formation porosity. The proposed method of finding porosity uses inductive logging technology and is an alternative to the method based on the mixing formulae.

Introduction

One of the key problems of borehole logging is finding porosity. For example, there is a borehole method of finding porosity using inductive logging, based on the Archie formula (Karpov et al., 2014; Makarov et al., 2012; Eltsov et al., 2011; Makarov et al., 2010; Gladkikh et al., 2009; Makarov et al., 2009; Antonov et al., 2009; Eltsov et al., 2009; Makarov et al., 2008). The main issues with this method are primarily due to the Archie formula itself. Another example is the method based on the mixing formulae. It originated back in the times of Maxwell. The basis for the method is the statement regarding the relationship between complex dielectric permittivity of the dielectric composite material and complex dielectric permittivity of

homogeneous infinite sub-systems. As this method is fairly popular (e.g., see (Seleznev et al., 2004)), let us briefly summarized the issues with it. Often, the CRIM formula is identified (Seleznev et al., 2004). It should be noted that the Brueggemann formula (Seleznev et al., 2004; Bruggeman, 1935) provides a result that is just as good. It should be noted that the physics behind the mixing formulae is the Maxwell-Wagner polarization due to migrant currents in the volumes of the sub-systems under study. It is not obvious that this polarization mechanism occurs in water-saturated porous rocks within a wide enough frequency range of the electromagnetic field. If we substitute complex dielectric permittivities of homogeneous sub-systems to the CRIM formula, it will be easy to see that the Havriliak-Negami polarization, while holding true for water-saturated systems (Levitskaya, 1984; Levitskaya et al., 1984; Levitskaya et al., 1990; Levitskaya et al., 1996), does not hold true here. Furthermore, the spectrum of complex dielectric permittivity generated by the CRIM formula in the low-frequency domain has a singularity. There are five unknown parameters in the two-component system, but we can only measure two of them at a fixed frequency. The unknowns are: bulk fraction of components, real parts of dielectric permittivity of the sub-systems, and conductance of the sub-systems with respect to direct current. The last two values cannot be found in a handbook. Only the real and imaginary parts of complex dielectric permittivity of the dielectric composite material can be measured at a fixed frequency. It would be possible to use other frequencies if the CRIM formula generated the Havriliak-Negami spectrum, but it does not.

In (Eltsov, 2014), a novel method of finding formation porosity for rocks saturated with water and oil was proposed. According to laboratory data (Levitskaya, 1984; Levitskaya et al., 1984; Levitskaya et al., 1990; Levitskaya et al., 1996), the frequency dependence of complex dielectric permittivity of the rock formation saturated with a mixture of water and oil is described by the Havriliak-Negami curve:

$$\varepsilon(\omega) - \varepsilon' \quad i\varepsilon'' - \varepsilon_{\infty} \quad \frac{\Delta\varepsilon}{\left[1 + (i\omega\tau)^{-\alpha}\right]^{\beta}}, \tag{1}$$

where ε is complex dielectric permittivity, ε_{∞} is permittivity in the high-frequency limit, $\Delta\varepsilon$ is the degree of polarization, τ is the relaxation time, α and β are polarization parameters. In (Eltsov, 2014), it is shown that one can find formation porosity and water-oil ratio if the spectrum of complex dielectric permittivity is known, i.e., if the polarization parameters are known. The procedure is as follows. Polarization parameters (α, β) determine ν (Chelidze, 1977) in accordance with the formula deduced from (1):

$$\nu - \operatorname{tg}\left[\frac{(1-\alpha)\pi}{4}\right]\chi(\beta), \qquad \chi(\beta) = 2\left[\sin\left(\frac{\pi\beta}{2(1+\beta)}\right)\right]^{-1/\beta}. \tag{2}$$

After that, porosity φ is found in accordance with the formula $\varphi = 1 - 4(\operatorname{arct}\nu)/\pi$, while oil saturation is determined by $\eta = 1 - \alpha/\varphi$. It should be noted that this parameter will be the same for the same sample at different water and oil ratios in the pores. The proposed procedure of finding porosity is verified using a series of additional laboratory experiments (Eltsov, 2014). Fig.1 shows the spectrum for sandstone with porosity of 14.1%, saturated with a solution of table salt, saline concentration 15 g/L (Levitskaya et al., 1990).

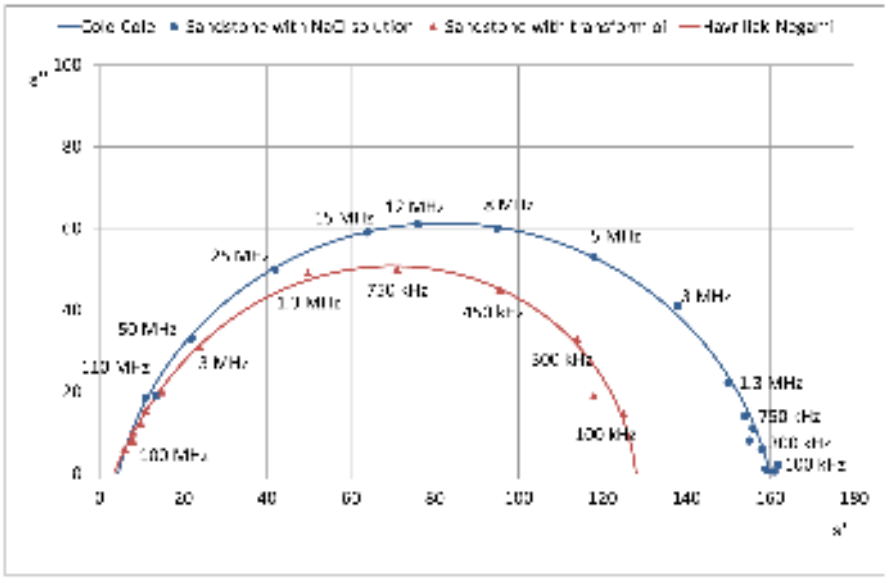

Figure 1—The spectrum of complex dielectric permittivity for sandstone (14.1% porosity) saturated with water (blue curve) and a mixture of water and oil (red curve) with the oil content of 7.6% of pore volume (Levitskaya et al., 1990)

As it follows from the Cole-Cole polarization dependence that holds true for water-saturated media (the Havriliak-Negami polarization $\beta = 1$), every set of three measurements of the spectrum of complex dielectric permittivity corresponding to different frequencies of the electromagnetic field can be matched to corresponding polarization parameters. Obviously, each measurement in Levitskaya's data reported in (Levitskaya et al., 1990) contains some random error, therefore every set of three measurements corresponding to different frequencies correspond to their respective polarization parameters. A bar graph for the parameter α illustrating this (when there is no oil in the pores, α corresponds to the value of porosity) is shown in Fig. 2. It should be noted that the maximal distribution value of corresponds to the value of porosity, whereas the difference between the maximal value of porosity corresponding to measured dielectric permittivity in a capacitor connected in a semi-stationary circuit and that of the direct laboratory measurement of porosity is less than 1%.

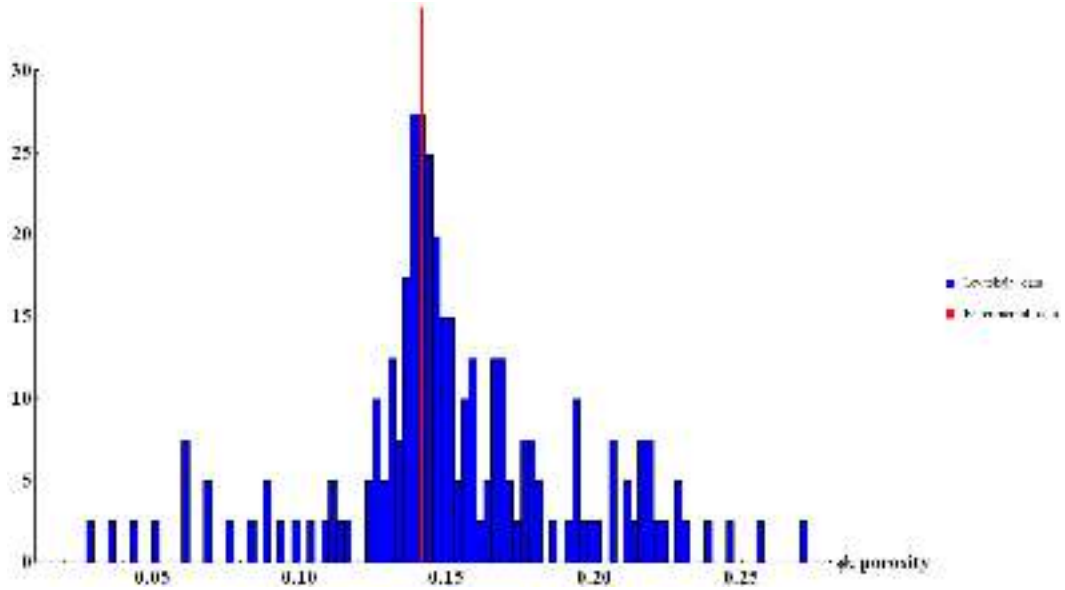

Figure 2—The bar graph of porosity distribution based on the spectrum of complex dielectric permittivity for water-saturated sandstone with 14.1% porosity (blue), [14]

Borehole measurements of porosity by a borehole inductive logging tool have their own type of error. It appears beneficial to study the ratio between the maximal value in the bar graph of polarization parameters based on complex dielectric permittivity values obtained via borehole inductive logging on one hand, and a known value of formation porosity obtained via core analysis in the lab. As one can see from Fig.1, we have excellent agreement between the maximal value of polarization parameter distribution and the exact value of porosity obtained in the lab; this may prove to become the basis for a high-precision method of finding porosity downhole using borehole inductive logging.

Forward Problem

Inductive logging is used for finding dielectric permittivity under downhole conditions (Antonov, 1979). The complex value of dielectric permittivity is found from the attenuation of the plane component of the magnetic field and the corresponding attenuation of the phase difference.

A point-like magnetic dipole $\mathbf{M} = (0, 0, M_z)$ is placed at the borehole axis. It excites the electromagnetic field which is harmonic in time and propagates in the borehole and in the rock saturated with water and oil, surrounding the borehole. The magnetic field harmonic in time is measured by means of several receivers spaced at a certain distance between each other and from the source. The medium is considered non-magnetic. The value of the magnetic field is used in calculation of for the formation, in accordance with the Maxwell-Fourier equations representing time dependence:

$$\begin{aligned} &\mathrm{rot}\,\mathbf{E} = i\omega\mu_0\mathbf{H}, \qquad \mathrm{div}\,\mathbf{E} = 0, \\ &\mathrm{rot}\,\mathrm{rot}\,\mathbf{H} - \mathrm{k}^2\,\mathbf{H} = 0, \qquad \mathrm{div}\,\mathbf{H} = 0, \end{aligned} \tag{3}$$

$$k^2 = -\omega^2\mu_0\varepsilon_0\varepsilon = -\omega^2\mu_0\varepsilon_0\left(\varepsilon' - i\varepsilon''\right) = -\omega^2\mu_0\varepsilon_0\left(\varepsilon_\infty + \frac{\Delta\varepsilon}{1+(i\omega\tau)^{1-\alpha}}^{\beta}\right).$$

We are considering the frequency domain of the electromagnetic field, where the input into the imaginary part of complex dielectric permittivity with respect to direct current may be neglected.

Let us consider an axially symmetrical model of a borehole with discrete identification of the invaded zone via dielectric permittivity: borehole radius is $R1$, invaded zone radius is $R2$; k_1, k_2, k_3 are values of k corresponding to mud, invaded zone, and formation, respectively (Fig. 3).

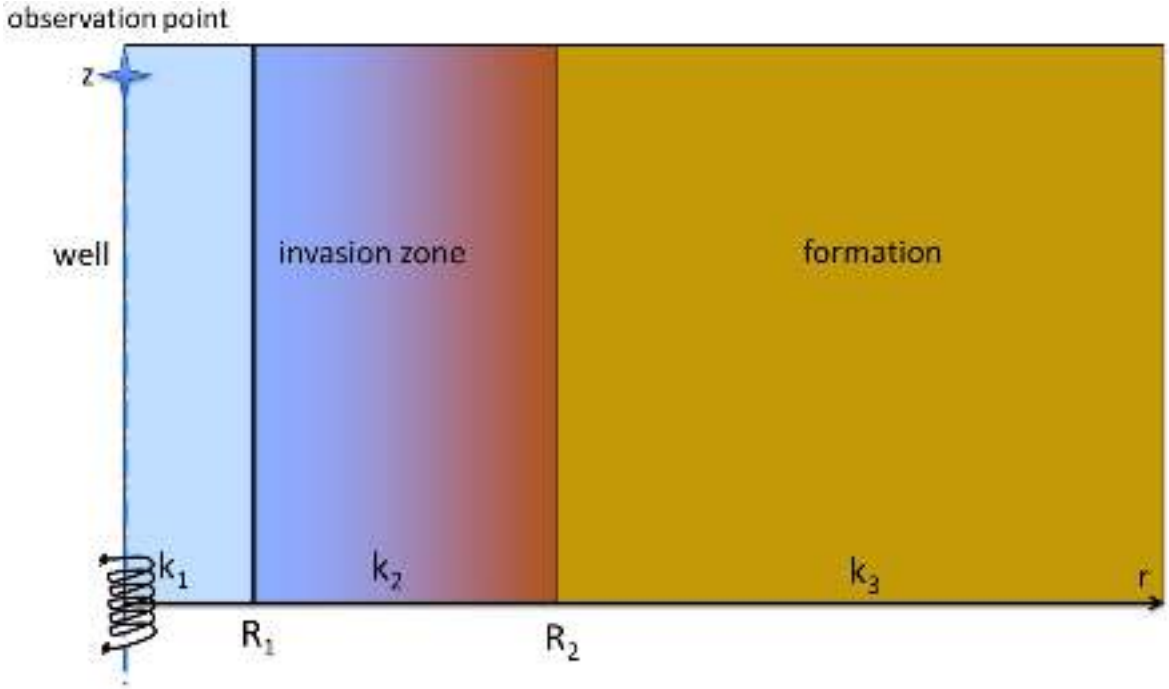

Figure 3—The borehole model

The expression for the magnetic field H_z on the borehole axis as in, for example, (Chelidze et al., 1977):

$$H_z = \frac{M_z}{2\pi}\frac{1+kz}{z^3}\exp(-kz)+\frac{2}{\sqrt{2\pi}\mu_0}\int_0^{\infty}\sqrt{k_z^2+k_1^2}\,\beta_1\cos(k_z z)\,dk_z\,. \tag{4}$$

The Fourier transform of (4) with respect to the longitudinal coordinate z can be presented as the following formula:

$$\tilde{H}_z = \frac{M_z}{4\pi}\sqrt{\frac{2}{\pi}}\left(k_z^2+k_1^2\right)\left[\ln\left(\frac{r}{2}\sqrt{k_z^2-k_1^2}\right)+\gamma\right]+\frac{\sqrt{k_z^2+k_1^2}\,\beta_1}{\mu_0}, \tag{5}$$

where γ is the Euler constant, r is the distance to the borehole axis, β_1 can be expressed via model parameters:

$$\beta_1 = \frac{\mu_0 M_z}{4\pi}\sqrt{\frac{2}{\pi}}\sqrt{k_z^2+k_1^2}\cdot\frac{KI(R_1,k_1,k_2)\,KK(R_2,k_2,k_1)+KK(R_1,k_1,k_2)\,KI(R_2,k_1,k_2)}{II(R_1,k_1,k_2)\,KK(R_2,k_2,k_1)\quad KI(R_1,k_2,k_1)\,KI(R_2,k_2,k_2)}, \tag{6}$$

$$KI(r,k_1,k_2) = \begin{vmatrix} K_0\left(r\sqrt{k_z^2+k_1^2}\right) & I_0\left(r\sqrt{k_z^2-k_2^2}\right) \\ K_2\left(r\sqrt{k_z^2+k_1^2}\right) & I_2\left(r\sqrt{k_z^2-k_2^2}\right) \end{vmatrix}, \tag{7}$$

$$KK(r,k_1,k_2) = \begin{vmatrix} K_0\left(r\sqrt{k_z^2+k_1^2}\right) & K_0\left(r\sqrt{k_z^2+k_2^2}\right) \\ K_2\left(r\sqrt{k_z^2+k_1^2}\right) & K_2\left(r\sqrt{k_z^2+k_2^2}\right) \end{vmatrix}, \tag{8}$$

$$\Pi(r,k_1,k_2)=\begin{vmatrix} I_0\left(r\sqrt{k_2^2+k_1^2}\right) & I_0\left(r\sqrt{k_2^2-k_3^2}\right) \\ I_2\left(r\sqrt{k_2^2+k_1^2}\right) & I_2\left(r\sqrt{k_2^2-k_3^2}\right) \end{vmatrix}. \tag{9}$$

Let us find the asymptotic expansion of the field on the borehole axis, and to this end, let us expand the Fourier image of the magnetic field into a series with respect to the powers of the small parameter $R_2\sqrt{k_1^2+k_3^2}$. Below, see the expansion of magnetic the field taking into account the term of the first degree of smallness $(\bar{H}_z)_1$:

$$(\bar{H}_z)_1 \approx \frac{M_z}{4\pi}\sqrt{\frac{2}{\pi}}\left\{\left(k_2^2+k_1^2\right)\ln\left(\frac{r}{R_1}\right)+\ln\left[\frac{R_1}{R_2}\right]-\left(k_2^2+k_3^2\right)\left(\ln\left[\frac{R_2}{2}\sqrt{k_2^2+k_3^2}\right]+\gamma\right)\right\}. \tag{10}$$

The next term of the expansion has the following form:

$$\begin{aligned}(\bar{H}_z)_2 \approx \frac{M_z}{4\pi}\sqrt{\frac{2}{\pi}}\Bigg\{&\frac{1}{2}R_1^2\left(k_2^2-k_1^2\right)\ln\left[\frac{R_1}{R_2}\right]+\\ &+\left(\frac{1}{2}R_1^2\left(k_2^2-k_1^2\right)+\frac{1}{2}R_2^2\left(k_3^2-k_2^2\right)\right)\left(k_2^2-k_3^2\right)\left(\ln\left[\frac{R_2}{2}\sqrt{k_2^2+k_3^2}\right]+\gamma\right)+\\ &+\frac{R_1^2}{4}\left(\left(k_2^2-k_1^2\right)^2-\left(k_2^2+k_3^2\right)^2\right)-\frac{R_2^2}{4}\left(\left(k_2^2+k_3^2\right)^2-\left(k_2^2+k_3^2\right)^2\right)\Bigg\}.\end{aligned} \tag{11}$$

The inverse Fourier transform of (10) and (11) yield the asymptotic field H_z taking into account the terms of the first degree of smallness:

$$(H_z)_1 \approx \frac{M_z}{2\pi}\frac{(1+k_3z)}{z^3}\exp\left[-k_3z\right]. \tag{12}$$

The next term of the expansion has the following form:

$$(H_z)_2 \approx \frac{M_z}{2\pi}\left\{\frac{1}{2}R_1^2\left(k_2^2-k_1^2\right)+\frac{1}{2}R_2^2\left(k_3^2-k_2^2\right)\right\}\frac{(1+k_3z)}{z^3}\exp\left[-k_3z\right]. \tag{13}$$

The total field taking into account the terms of the first and second degrees of smallness has the following form:

$$H_z \approx (H_z)_1+(H_z)_2 \approx \frac{M_z}{2\pi}\left\{1+\frac{1}{2}R_1^2\left(k_2^2-k_1^2\right)-\frac{1}{2}R_2^2\left(k_3^2-k_2^2\right)\right\}\frac{(1+k_3z)}{z^3}\exp\left[-k_3z\right]. \tag{14}$$

Inverse Problem

Two schemes of solving the inverse problem are considered with respect to finding k_3 of the formation under study. The first scheme corresponds to the two-coil measurement circuit (Fig. 4).

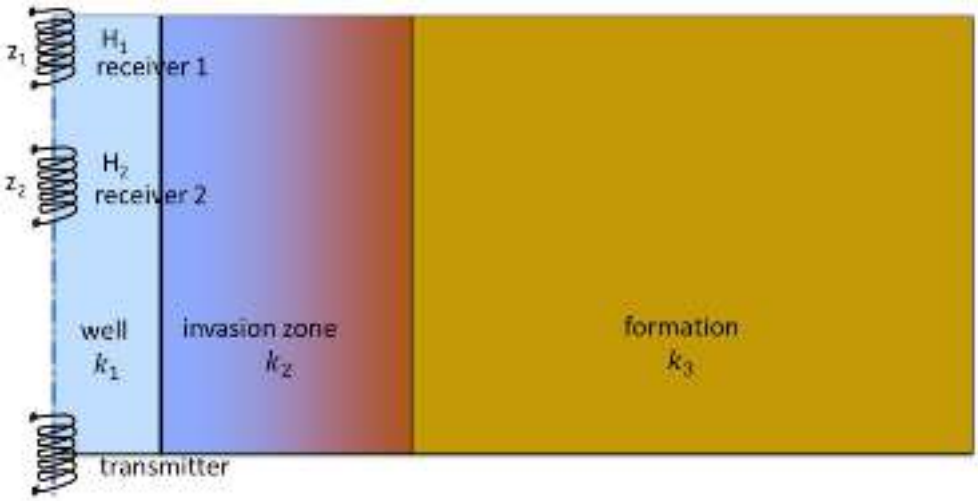

Figure 4—The two-coil measurement circuit. H1, H2, are results of measuring the magnetic field with coils located in points z1, z2

To find the wave number k_3, this scheme uses the expression for the asymptotic fields on the borehole axis (14). This expression contains a product of the parameters of the invaded zone and the borehole parameters. If the magnetic field measured by one receiver is divided by that measured by the other receiver, the inputs of the invaded zone and borehole are eliminated and the resulting expression depends only on the formation parameters (15).

$$\frac{H_1 z_1^3}{H_2 z_2^3} - \frac{1 + k_3 z_1}{1 + k_3 z_2} \exp[k_3 (z_2 - z_1)], \tag{15}$$

where magnetic fields H_1, H_2 denote the longitudinal magnetic field in the neighborhood of Receiver 1 and Receiver 2.

Equation (15) has several roots which cannot be expressed in elementary functions. To find k3, equation (15) was solved numerically, and the criteria of root selection were as follows:

$$\mathrm{Re}[\varepsilon] - \varepsilon' > 0, \qquad \mathrm{Im}[\varepsilon] - \varepsilon'' < 0. \tag{16}$$

The need to have a three-coil circuit for measurements (see Fig. 4) is conditioned by the fact that the small parameter used increases with frequency:

$$R\sqrt{k_x^2 + k_n^2} \approx R\omega\sqrt{\mu_0 \varepsilon_0 \varepsilon}. \tag{17}$$

In the MHz domain, with typical values of dielectric permittivity of the invaded zone, the accuracy of asymptotic expansion taking into account the terms of the second degree of smallness, drastically drops, and therefore, so does the accuracy of the two-coil circuit.

The following text discusses a problem of finding formation parameters based on measurements of the longitudinal magnetic field at the borehole axis with a higher accuracy than the two-coil circuit would provide. Let us consider the borehole radius R_1, mud parameters, and therefore, parameter k_1 known. The complex formation parameter k_3 and its value in the invaded zone k_2, as well as the invaded zone radius, remain unknown (5 values total). Therefore, for the inversion in the model under study to be accurate, we need to measure the magnetic field in three points. Taking into account the real and imaginary parts of the field, we arrive at six equations, which are sufficient for finding five unknowns.

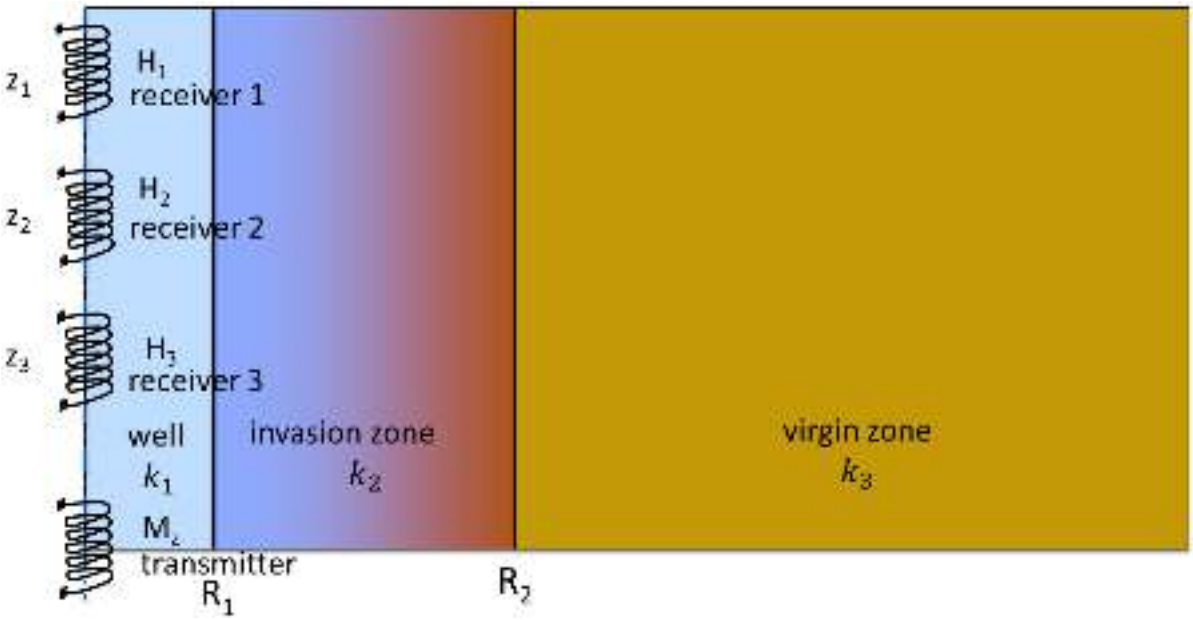

Figure 5—The diagram of formation parameter measurements. H1, H2, H3 are the results of measurement of the longitudinal magnetic field using the coils located in points z1, z2, z3 at the axis of symmetry

The following algorithm was used for inversion:

1. Find the first approximation k_3 from the asymptotic ratio for the second and third coils using equation (15).
2. Using the asymptotic equation (14) for the first coil, find the approximated dependence $k_2(R_2)$.

$$\frac{1}{2}R_1^2(k_2^2-k_1^2)+\frac{1}{2}R_2^2(k_3^2-k_2^2)-\frac{2\pi H_z z_1^3}{M_z(1+k_1 z_1)}\exp[k_3 z_1]=1. \tag{18}$$

3. Substituting the approximated dependence $k_2(R_2)$ (18) into the exact expression (4) for the third coil, we arrive at an equation for R_2, which can be solved numerically.

$$H_3=\frac{M_z}{2\pi}\frac{1+k_1 z_3}{z_3^3}\exp(-k_1 z_3)+\frac{2}{\sqrt{2\pi\mu_0}}\int_0^\infty\sqrt{k_z^2+k_1^2}\,\beta(k_2(R_2),k_3)\cos(k_z z)\,dk_z. \tag{19}$$

   As a result, we find approximated values of k_2 and R_2.
4. The approximated values of k_2, k_3 and R_2 found are used as initial approximations for the multi-dimensional optimization:

$$\frac{|H_z(z_1)-H_1|^2}{|H_1|^2}+\frac{|H_z(z_2)-H_2|^2}{|H_2|^2}+\frac{|H_z(z_3)-H_3|^2}{|H_3|^2}\to 0. \tag{20}$$

where $H_z(z)$ is the exact expression for the magnetic field at the borehole axis (4).

Numerical experiment

A model of a probe is considered in the 100 kHz to 30 MHz frequency range. The distance between the receivers and the source of the harmonic electromagnetic signal varies from 4 m (for 100 kHz) to 0.5 m (for 30 MHz).

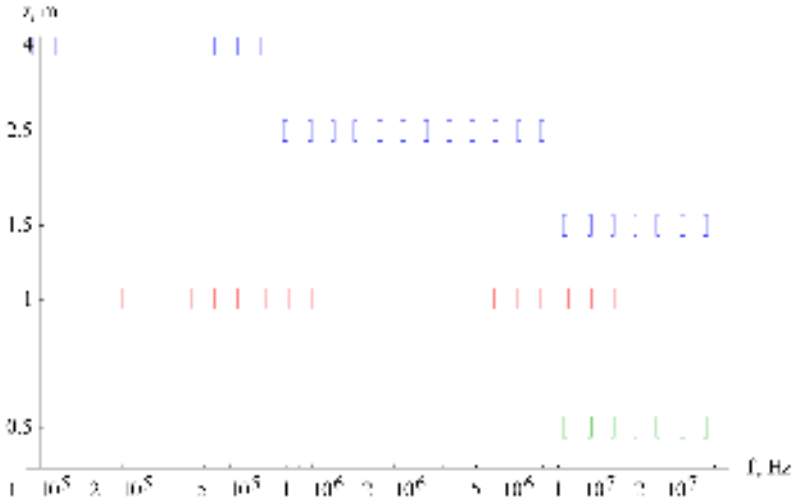

Figure 6—The distance between the receivers and the source of the electromagnetic signal as function of frequency. At frequencies under 7 MHz, the two-coil measurement circuit was used and at frequencies over 7 MHz, the three-coil measurement circuit

When processing the signals and finding the measurement error, it was assumed that the ratio between the amplitudes of the signal in the borehole and in air in the same point of space, for the same source, satisfies the following condition:

$$\frac{H}{H_{воздух}} = 10^{Att/20} e^{i Ph \pi/180} \tag{21}$$

Here, *Att* denotes attenuation and *Ph* denotes the phase shift during signal attenuation. As a result, we have a known amplitude ratio for two fields related to two different points in space (z_1,z_2)

$$\frac{H}{H_2} = \left(\frac{z_1}{z_2}\right)^3 10^{(Att_1 - Att_2)/20} e^{i(Ph_1 - Ph_2)\pi/180}.$$

Formula (21) is convenient when one needs to introduce the accuracy of measuring the amplitude of the received signal. When recovering the values of complex dielectric permittivity, the measurement error (the measured signal) was modeled by adding random noise:

$$\begin{aligned} Att_m &= Att + \delta Att \cdot N_1, \\ Ph_m &= Ph + \delta Ph \cdot N_2. \end{aligned} \tag{22}$$

where Att_m and Ph_m are "measured signals," N_1 and N_2 are two independent random numbers from the normal distribution with the mathematical expectation of 0 and the standard deviation of 1. Here, *Att, Ph* correspond to the fields calculated for the exact value of complex dielectric permittivity corresponding to the Havriliak-Negami polarization. When introducing an error to the field amplitudes, we determine polarization parameters with an error characteristic of the inductive measurement procedure and borehole accuracy of field readings. The values of the measurement errors δAtt and δPh were 1.0% of the value of the signal (23):

$$\begin{aligned} \delta Att &= \begin{cases} 1\% \cdot Att, & \text{if} \quad Att > 1dB \\ 0.01dB, & \text{else} \end{cases} \\ \delta Ph &= \begin{cases} 1\% \cdot Ph, & \text{if} \quad Ph > 10^\circ \\ 0.1^\circ, & \text{else} \end{cases} \end{aligned} \tag{23}$$

In such an error model, the accuracy of dielectric permittivity measurement depends on frequency. Let us find this dependence for the two-coil measurement circuit. To this end, let us express equation (15) via the phase difference and attenuation:

$$10^{\frac{Att_1 - Att_2}{20}} \exp\left(i\frac{\pi(Ph_1 - Ph_2)}{180}\right) = \frac{1 + k_1 z_1}{1 + k_2 z_2}\exp(ik_1(z_2 - z_1)). \tag{24}$$

Let us calculate the logarithmic differential of the left- and right-hand sides of the equation (24).

$$\frac{\ln(10)}{20}(\delta Att_1 - \delta Att_2) + i\frac{\pi}{180}(\delta Ph_1 - \delta Ph_2) = (z_2 - z_1)d\frac{\delta k^2}{2k}, \tag{25}$$

$$d = 1 - \frac{1}{(1 - kz_1)(1 + kz_2)},$$

where δAtt_1, δPh_1 are errors of phase difference and attenuation in the first coil, δAtt_2, δPh_2 are errors of phase difference and attenuation in the second coil.

Substituting expression (3) linking the wave number with dielectric permittivity into (25), we obtain the error of measuring dielectric permittivity expressed via the errors of phase difference and attenuation.

$$\delta\varepsilon = -\frac{2k}{\omega^2\mu_0\varepsilon_0}\frac{\ln(10)(\delta Att_1 - \delta Att_2)/20 + i\pi(\delta Ph_1 - \delta Ph_2)/180}{(z_2 - z_1)d}. \tag{26}$$

Assuming the measurement errors are statistically independent and the standard deviations are the same in the first and second coil, we can use equation (26) to express the accuracy of measuring the real and imaginary parts of dielectric permittivity (27):

$$\frac{\mathrm{Re}[\delta\varepsilon]}{\mathrm{Re}[\varepsilon]} = \frac{\sqrt{2d_1^2 + 2d_2^2}}{\mathrm{Re}[k^2]|d_3|^2}, \qquad \frac{\mathrm{Im}[\delta\varepsilon]}{\mathrm{Im}[\varepsilon]} = \frac{\sqrt{2d_1^2 + 2d_2^2}}{\mathrm{Im}[k^2]|d_3|^2}, \tag{27}$$

$$d_1 = \frac{\ln(10)}{20}\delta Att\ \mathrm{Re}\left(\frac{z_2 - z_1}{2k}d\right), \qquad d_2 = \frac{\pi}{180}\delta Ph\ \mathrm{Im}\left(\frac{z_2 - z_1}{2k}d\right), \qquad d_3 = \frac{z_2 - z_1}{2k}d.$$

Dielectric permittivity of rock samples saturated with a mixture of oil and water was measured in the laboratory using the impedance method (Table 1). These data were used as dielectric permittivity of the formation, together with corresponding Havriliak-Negami polarization parameters.

Table 1—Laboratory samples: porosity listed was measured in the laboratory by mechanical removal of fluid out of samples

Sample No.	Rock type	Porosity	Oil Saturation					
5-02	sandstone	22.9%	0%	10%	20%	30%	40%	50%
15-02	sandstone	15.5%	0%	10%	20%	30%	40%	50%
53-02	sandstone	18%	0%	10%	20%	30%	40%	50%
64-02	sandstone	21%	0%	10%	20%	30%	40%	50%
107-02	sandstone	10.3%	0%	10%	20%	30%	40%	50%
333-94	carbonate	18.65%	0%	10%	20%	30%	40%	50%
334	carbonate	18.96	0%	10%	20%	30%	40%	50%
339	carbonate	20.5	0%	10%	20%	30%	40%	50%
344-94	carbonate	21.8	0%	10%	20%	30%	40%	50%
3617	carbonate	9.8	0%	10%	20%	30%	40%	50%

Borehole parameters in the model: the radius is 0.1 m, the borehole is filled with OBM (Patil et al, 2010) (dielectric permittivity of mud ε_b was considered equal 10—i0.18). Parameters of the invaded zone (skeleton type, porosity) were considered to be the same as those of the formation under study, but for

different ratios of oil and water. Oil saturation of the invaded zone was set to 50%, whereas it was 30% of the pore volume in the formation under study. The radius of the invaded zone was set to 0.4 m.

A series of numerical experiments was performed to study the accuracy of finding the dispersion curve, polarization parameters, porosity, and oil saturation. As an example, let us consider a sandstone sample with the following parameters: porosity = 18%, oil saturation = 30%, $\varepsilon_\infty = 11.2$, $\Delta\varepsilon = 369$, $t = 1.2$ MKC, $\alpha = 0.13$, $\beta = 0.83$. The dispersion curves of the sample were recovered from the data with artificial noise added, taking into account the invaded zone (Fig. 7). The dispersion curves were recovered from "measured data" Att_m and Ph_m. The squared inverse value of the measurement accuracy of dielectric permittivity with the two-coil circuit (27) served as weight functions G_{Re}, G_{Im}:

$$G_{Re} = \left(\frac{\mathrm{Re}[\varepsilon]}{\mathrm{Re}[\delta\varepsilon]}\right)^2, \qquad G_{Im} = \left(\frac{\mathrm{Im}[\varepsilon]}{\mathrm{Im}[\delta\varepsilon]}\right)^2. \tag{28}$$

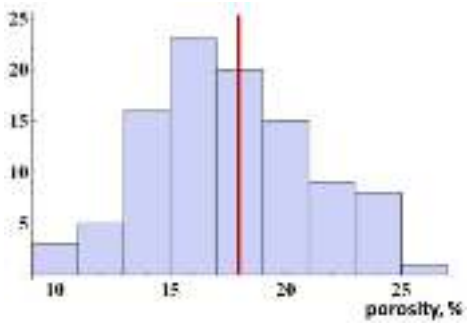

Figure 7—Porosity distribution for Sample No. 53, recovered from the data with artificial noise added. Red lines correspond to the exact values

As one can see, the accuracy of dispersion curve recovery in the MHz domain is better than in the kHz domain, the reason being low accuracy of measuring the magnetic field anomaly in the kHz domain, due to insufficient spacing between the receivers and the source for this frequency range. Porosity values for this sample were calculated based on the dispersion curve data with artificial noise added. Approximately 100 numerical experiments were performed (100 realizations of artificial noise when modeling borehole measurements); each realization corresponds to one computed value of porosity. As a result of this series of numerical experiments, porosity distributions were obtained as shown in Fig. 8 for Sample No. 53. For the sample presented, the standard deviation (statistical error) for porosity was 20.0%. It should be noted that the maximum of porosity distribution is 16%, while true porosity is 18%. In this case, the measurement error is 11%.

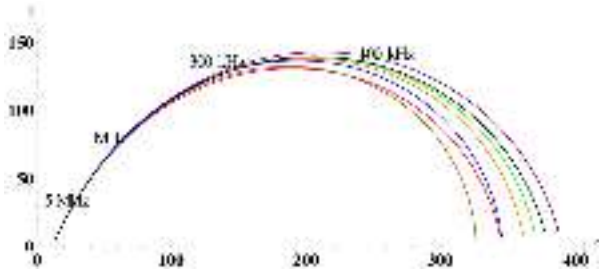

Figure 8—The spectrum of dielectric permittivity and porosity distribution for Sample No. 53, recovered from the data with artificial noise added. Red lines correspond to the exact values

Fig. 9 shows a bar graph for Sample No. 64, sandstone, oil saturation 30% of pore space with porosity measured in the lab being 21%. The maximum of the bar graph is 21%. The error is less than 1%. It should be noted that for this sample, the relaxation time for the polarization process is 1.2 μs, whereas the relaxation time for Sample No. 64 is 0.31 μs. The recovery error for the polarization curve appears to drop in the low-frequency domain, as one can observe from Fig. 10.

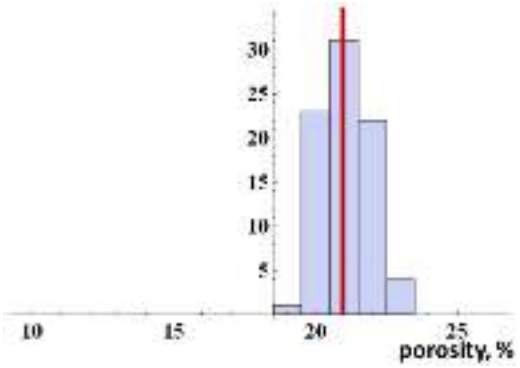

Figure 9—Porosity distribution for Sample No. 64, recovered from the data with artificial noise added. Red lines correspond to the exact values

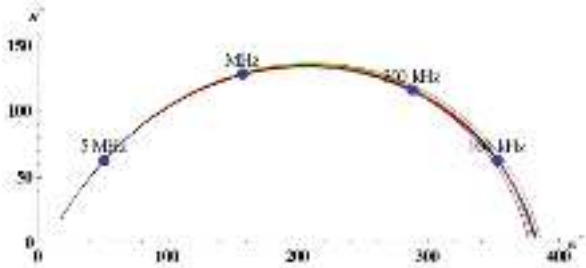

Figure 10—Recovered spectra of dielectric permittivity for Sample No. 64 for different versions of artificial noise

Fig. 11 demonstrates the ″interim″ sample with the relaxation time of 0.85 μs (Sample No. 333).

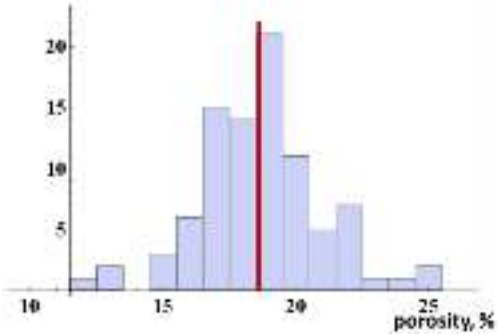

Figure 11—Porosity distribution for Sample No. 333, recovered from the data with artificial noise added. Red lines correspond to the exact values

Porosity measured in the lab is 18.6%, the maximum of the porosity distribution is 19%. Fig. 12 demonstrates dielectric spectra recovered for this sample. Thus, with a decrease of characteristic relaxation times in the Havriliak-Negami polarization, the accuracy of finding porosity from the maximum of its distribution curves improves drastically. The samples shown (No. 333, No.54, No.63) were saturated

with distilled water. To improve the accuracy of porosity measurements, it is important to work with sample whose relaxation time is small. Fig. 13 shows the relaxation time as function of salinity for each value of porosity (Levitskaya, 1996).

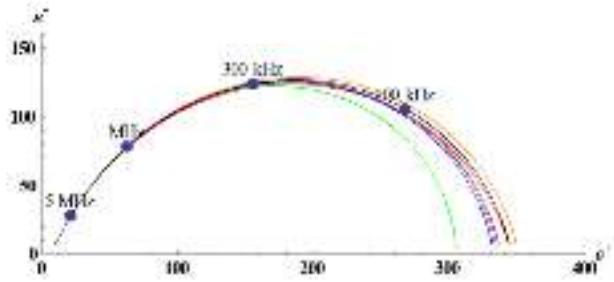

Figure 12—Recovered spectra of dielectric permittivity for Sample No. 333 for different versions of artificial noise

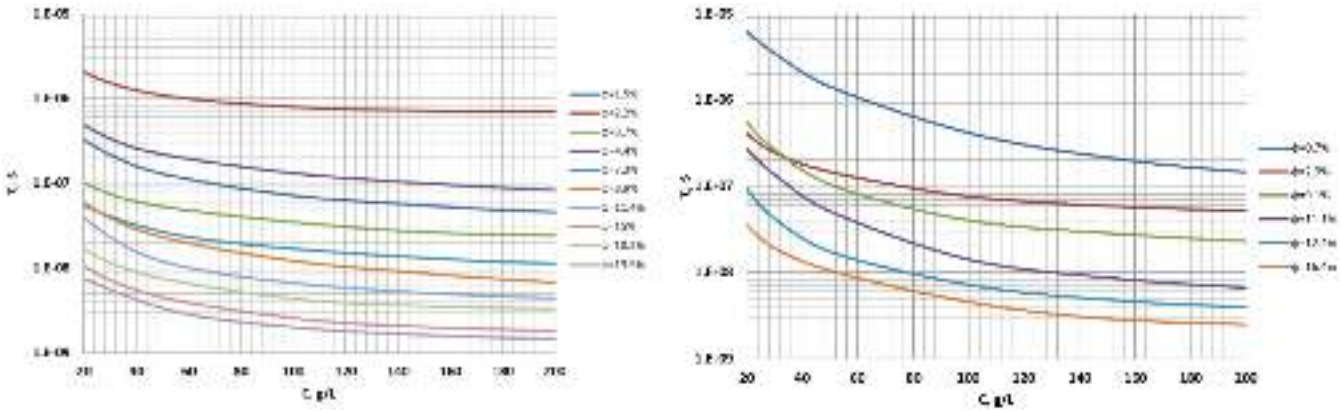

Figure 13—The relaxation time curves at different values of porosity in the Havriliak-Negami polarization for dolomites (Levitskaya, 1984) (a) and sandstones (Levitskaya, 1990) (b)

It should be noted that even for porosity of 2.9%, the error of finding porosity via inductive borehole measurements is less than 1%.

Conclusion

The present paper describes a new method of inductive borehole measurement of formation porosity, for the formation saturated with water and oil. Two known methods of inductive borehole measurement of porosity are mentioned. The weaknesses of these methods are described. The key advantages of the new method of measuring porosity are described, it being free from the issues typical of the two inductive borehole methods mentioned above.

1. Advantages of the new method include:
   a. There is no need to know dielectric permittivities of the sub-systems constituting the dielectric composite material;
   b. There is no need to know salinity of the saturating fluid in the pores;
   c. There is no need to know specific mixing formulae corresponding to lithology under study;
   d. There is no need to use the Archie formula.
2. Laboratory measurements of polarization parameters of the Havriliak-Negami spectrum of complex dielectric permittivity enable us to find porosity of a rock sample saturated with water and oil, with its characteristic measurement error. The polarization parameter distribution curve has a

maximum. This maximum determines sample porosity with no ambiguity.

3. The inductive electromagnetic borehole measurement of the spectrum of complex dielectric permittivity has its own characteristic measurement error as well. The polarization parameter distribution spectrum has a maximum. This maximum determines formation porosity.
4. The difference between the maximum of the polarization parameter (from the spectrum of values conditioned by the measurement error) and formation porosity decreases with the increase of the characteristic relaxation time for the dielectric polarization of the medium saturated with a mixture of water and oil.
5. For real rocks in the field, with salinity of the saturating fluid being 30 g/L, the measurement error for porosity when using the method proposed in the present paper does not exceed 1% if the amplitudes of the magnetic fields are measured with inductive borehole tools with the accuracy of 1%.

Nomenclature

α = polarization parameter of Havriliak-Negami curve,
β = polarization parameter of Havriliak-Negami curve,
β_1 = function used in the calculation of the magnetic field on the axis of the well, depends on the model parameters,
γ = Euler-Mascheroni constant, ≈ 0.577,
$\Delta\varepsilon$ = polarization level,
δAtt = attenuation measurement error of electromagnetic waves in a borehole, dB,
δPh = phase difference measurement error of electromagnetic waves in a borehole, °,
δAtt_i = attenuation measurement error on i_{th} receiver, dB,
δPh = phase difference measurement error on i_{th} receiver, °,
$\delta\varepsilon$ = permittivity measurement error,
ε = complex permittivity,
ε_0 = permittivity of free space, $\approx 8.854 \cdot 10^{-12}$F/m,
ε_b = permittivity mud,
ε' = real part of perπ complex permittivity,
ε'' = imaginary part of complex permittivity,
ε_∞ = the permittivity at the high frequency limit,
η = oil suturation, %,
ν = parameter the sample (unchanged at different ratios of water and oil in the pores),
π = mathematical constant $\pi \approx 3.1415$,
μ_0 = permeability of free space, $4\pi \cdot 10^{-7}$ H/m,
τ = the characteristic relaxation time, s,
φ = porosity, %,
ω = the angular frequency, rad/s,
Att = attenuation of electromagnetic waves in a borehole, dB,
Att_i = attenuation on i_{th} receiver, dB,
Att_m = attenuation with added measurement error, dB,
d = coefficient used in calculating an absolute measurement accuracy of the formation permittivity,
d_i = coefficient used in calculating a relative measurement accuracy of the formation permittivity,
$\mathbf{E}$ = electric field, V/m,
G_{Re} = the residual weight function of the real part of the dielectric constant,

G_{Im} = the residual weight function of the imaginary part of the dielectric constant,
$\mathbf{H}$ = magnetizing field, A/m,
H_z = magnetizing field on borehole axis, A/M,
H_i = magnetizing field in i_{th} receiver,
$\tilde{H}$ = magnetizing field Fourier transform on Z axis, A,
$(H_z)_1$ = the first term of the asymptotic expansion of the magnetizing field, A/m,
$(H_z)_2$ = the second term of the asymptotic expansion of the magnetizing field, A/m,
$(\tilde{H}_1)$ = the first order term in the expansion of the Fourier transform of the magnetizing field, A,
$(\tilde{H}_2)$ = the second order term in the expansion of the Fourier transform of the magnetizing field, A,
I_i = modified Bessel function of the first kind,
i = imaginary unit, $=\sqrt{-1}$,
K_i = modified Bessel function of the second kind,
k = wavenumber, m^{-1},
k_1 = wavenumber for mud, m^{-1},
k_2 = wavenumber for invasion zone, m^{-1},
k_3 = wavenumber for formation, m^{-1},
k_z = variable of Fourier transform on Z axis, m^{-1},
$\mathbf{M}$ = magnetic moment, $A \cdot m^2$,
M_z = component of the magnetic moment, $A \cdot m^2$,
N_i = a random number from normal distribution with standard deviation 1 and the mathematical expectation 0,
Ph = phase difference of the electromagnetic wave in the borehole, °,
Ph_i = phase difference of the electromagnetic wave on i_{th} receiver, °,
Ph_m = phase difference with added measurement error, °,
R_1 = well radius, m,
R_2 = invasion zone radius, m,
r = the distance from the axis of the borehole, m,
z = the height of the observation point to the transmitter, m,
z_i = coordinate of i_{th} receiver.

References

1. Antonov, Yu.N., and Burkov, V.G. 1979. *Regarding the Theory of High-Frequency Electro-Magnetic Logging of Boreholes with a Radially Uneven Invaded Zone*. Novosibirsk, Russia: Nauka.
2. Antonov, Yu., Kashevarov, A., Makarov, A., Wu, J., and Gladkikh, M. 2009. Computing True Formation Pressure Using Drilling and Logging Data, SPE 8th European Formation Damage Conference. Scheveningen, Netherlands.
3. Bruggeman, D.A.G. 1935. Berechnung verschiedener physikalischer Konstanten von heterogenen Substanzen // *Annalen der Physik*. **416**(7): 636–664.
4. Chelidze, T.L., Derevyanko, A.I., and Kurilenko, O.D. 1977. *Electric Spectroscopy of Heterogeneous Systems*. Kyev, USSR: Naukova Dumka.
5. Eltsov, I., Antonov, Yu., Makarov, A., and Kashevarov, A. 2011. Invaded Zone Evolution Reconstructed from Logging Data, SEG International Exposition Annual Meeting. Houston, USA.
6. Eltsov, T.I., Dorovsky, V.N., and Gapeev, D.N. 2014. Dielectric spectra of water-oil saturated porous media for the kHz range and determination of volume fractions of system components. *Russian Geology and Geophysics*. **55**(8): 1009–1018.

7. Eltsov, I., Kashevarov, A., Antonov, Yu., Makarov, A., and Gladkikh, M. 2009. Invaded Zone Forming According to the Field Experiment Data // *Karotazhnik Journal*. Tver, Russia.
8. Gladkikh, M., Makarov, A., LeCompte, B., Harvey, W., Antonov, Yu., and Halleck, P. 2009. Combining Prediction of Penetration Depth of Downhole Perforators with the Depth of Invasion, SPE 8th European Formation Damage Conference. Scheveningen, Netherlands.
9. Karpov, I., Makarov, A., and Eltsov, I. 2014. Oil Viscosity Impact on Invasion Zone Structure and Resistivity Measurements. SPE Russian Oil and Gas Conference & Exhibition. Moscow, Russia.
10. Levitskaya, Ts.M. 1984. Dielectric Relaxation in Rocks. *Earth Physics (Proceedings of USSR Academy of Science)*. **10**: 82–87.
11. Levitskaya, Ts.M., and Nosova, E.N. 1984. Analysis of Relaxation Parameters of Inter-Surface Polarization of Rocks // *Earth Physics (Proceedings of USSR Academy of Science)*. **10**: 88–93.
12. Levitskaya, Ts.M., and Palveleva, I.I. 1990. Influence of Hydrocarbons on Sandstone Dielectric Spectrum // *Earth Physics (Proceedings of USSR Academy of Science)*. **6**: 106–110.
13. Levitskaya, T.M., and Sternberg, B.K. 1996. Polarization Processes in Rocks 1. Complex Dielectric Permittivity Method // *RadioScience*. **31**(4): 755–779.
14. Makarov, A., and Eltsov, I. 2012. Interpretation of Resistivity Logs Based on Mathematical Modeling of Invaded Zone Evolution Taking into Account Mudcake Build-up, SPE Russian Oil and Gas Conference & Exhibition. Moscow, Russia.
15. Makarov, A., Kashevarov, A., and Eltsov, I. 2008. Formation Permeability Estimation from Microresistivity Logging Data, Interexpo Geo-Siberia. Novosibirsk, Russia.
16. Makarov, A., Kashevarov, A., and Eltsov, I. 2009. Caliper Data Interpretation Based on Hydrodynamic Modeling, EAGE International Geological and Geophysical Conference and Exhibition. Tyumen, Russia.
17. Makarov, A., Kashevarov, A., and Eltsov, I. 2010. Estimation of Formation Permeability Using Mudcake Parameters // *Karotazhnik Journal*. Tver, Russia.
18. Patil, P.A., Gorek, M., Folberth, M., Hartmann, A., Forgang, S., Fulda, C., and Reinicke, K.M. 2010. Experimental Study of Electrical Properties of Oil-Based Mud in the Frequency Range from 1 to 100 MHz. *SPE Drilling & Completion*. 380–390.
19. Seleznev, N., Boyd, A., Habasky, T., and Luthi, S.M. 2004. Dielectric Mixing Laws for Fully and Partially Saturated Carbonate Rocks. SPWLA 45th Annual Logging Symposium, June, 6-9. 1-14.